Magnesium Technology 2011
Edited by: Wim H. Sillekens, Sean R. Agnew, Neale R. Neelameggham, and Suveen N. Mathaudhu
TMS (The Minerals, Metals & Materials Society), 2011

DEVELOPMENT OF ZIRCONIUM-BASED CONVERSION COATINGS FOR THE PRETREATMENT OF AZ91D MAGNESIUM ALLOY PRIOR TO ELECTROCOATING

James Reck[1], Yar-Ming Wang[2], Hong-Hsiang (Harry) Kuo[2]
[1]United States Navy; 1240 Isaac Hull Ave. SE; Washington Navy Yard, DC, 20376, USA
[2]General Motors; GM R&D Center; Warren, MI, 48090, USA

Keywords: AZ91D, zirconia, conversion coating

Abstract
This work examines the use of hexafluorozirconic acid based solutions at concentrations from 0.025 M to 0.100 M and pH values of 2.0 to 4.0 for the creation of a zirconia-based conversion coating less than 1 micron thick to protect magnesium alloy AZ91D. Similar coatings have been found to give excellent protection for steel and aluminum alloys, but little research has been conducted on its application to magnesium. Work was performed to gain an understanding of the film formation mechanisms and related kinetics using x-ray photo-electron spectroscopy, scanning electron microscopy, and open circuit potential monitoring techniques. A design of experiments approach was taken to determine the effects of acid concentration, pH, and soak time on the corrosion properties both as-deposited and with an application of electrocoat. It was found that the application of the zirconia-based coating significantly increased corrosion resistance, and allowed for an acceptable e-coat application with excellent adherence.

Introduction
The use of Mg alloys for automotive applications has continued to increase in the industry, with hopes of increasing fuel economy by decreasing vehicle weight. Magnesium has a strength-to-weight ratio $^2/_3$ that of aluminum and ¼ that of iron while still exhibiting high thermal conductivity, high dimensional stability, good damping characteristics, and is easily recycled, making it one of the lightest structural metals available [1]. Magnesium, however, is currently limited in use due to a low resistance to corrosion. This issue can be addressed, to a limited extent, by alloying, but is more appropriately handled using a series of protective coatings.

The current automotive standard coating sequence for steel-based body structures involves a pre-treatment stage of phosphating prior to e-coat application. The phosphating process produces a conversion coating that assists in corrosion prevention by decreasing the active surface area of the metal available for corrosion reactions [2]. Some of the major issues with the phosphate process include sludge generation (which requires frequent desludging of process tanks in addition to expensive filters), the use of heated tanks requiring large amounts of energy, and a post phosphate sealing procedure to fill in the pores created during deposition [3]. Additionally, Mg dissolution in the traditional phosphate chemistries [4, 5] in conjunction with rising environmental restrictions and energy costs [3, 6, 7] are driving research efforts to find a cost efficient but equally protective coating process.

Several coating technologies have been researched to address the need for an Mg coating process that will provide cost effective corrosion protection. Popular methods include modifications of the phosphate process [4, 5, 8], Cr(III) conversion coatings [1], stannate conversion coatings [9], and cerium oxide conversion coatings [10, 11], but the emergence of ZrO_2-based nano-coatings have been of significant interest [2, 12-18]. These ZrO_2-based coatings have been well characterized on aluminum [7, 19-24] and steel [3, 7, 25-28], but significant work remains to be done on its use with magnesium. On aluminum and steel alloys, these coatings have been found to be very thin (e.g. <100 nm) [3, 6, 13, 24, 27], show acceptable corrosion protection up to 70 days of salt fog exposure [3, 20], and have been cited as providing "similar protection behavior as Zn and Fe phosphate coating" when combined with a layer of e-coat after deposition [3].

Experimental
Material and Sample Preparation. A single batch of die cast AZ91D test panels was sectioned into approximately 2"x4" coupons. The panels were polished using a series of 240, 320, 400, 600, and 1200 grit SiC sandpaper. All but the final sanding was performed using tap water for lubrication and dust removal.

The polished AZ91D plates were subjected to a pretreatment consisting of either an acid clean in 1wt% H_2SO_4 at 55°C followed by a 45°C DI water rinse (referred to as Ac or the acid clean) and/or an alkaline clean in 5wt% Na_2CO_3 followed by a DI water rinse (referred to as Alk or alkaline cleaning), all solutions at room temperature. The specimen was then immediately submerged in the prepared H_2ZrF_6 solution for the prescribed period of time.

If prescribed, the e-coat was applied with a prescribed voltage for a set time to attach the polymer chains to the nano-coated AZ91D plates. A post-deposition cure of 171°C for 25 minutes was used to reflow the polymers for a smoother, more adherent e-coat.

Solutions for the ZrO_2-based nano-coatings were prepared in 2 liter batches using a concentrated solution of 50 wt% hydrofluorozirconic acid (H_2ZrF_6) that was diluted to the desired concentration with DI water. All dilutions were specified by moles per liter (M) and prepared by weight. Titration to the desired pH was accomplished with concentrated NaOH solution.

E-coating was performed using a Darrah Electric 5-500 power supply which could supply a maximum of 500 V and 5 A, run under voltage control. The e-coat material used was a premixed solution of Dupont Cormax VI Gray.
Experimental Setup. Following initial coating studies, the general effectiveness of a ZrO_2-based nano-coating on Mg was examined using a design of experiments (DOE) regimen. The variables of interest were the concentration of H_2ZrF_6 (0.025, 0.050, and 0.100 M), solution pH (2,3, and 4), immersion time (30, 60, and 90 seconds), and surface pretreatment (alkaline or acid-alkaline). Given the large number of variables and the number of desired levels, a full factorial DOE (54 runs) was not feasible. So a Box-Behnken surface response, limited–sample DOE regimen was used (16 runs). The results of the DOE allowed for process optimization, resulting in a combination of factors that result in

the most desirable ZrO_2-based film.

Using the optimized ZrO_2-based nano-coating from the first DOE, a second DOE matrix was developed to optimize the deposition of the e-coat layer on top of the nano-coat. This regimen was designed as a full factorial matrix with voltage (150, 200, and 250 V) and time (1, 2, and 3 minutes). The results of the combined DOE results allowed the preparation of the best nano-coat plus e-coat bi-layer system on AZ91D possible within the design space studied for both DOEs for given the chosen optimization criteria.

Results and Discussion

The research was conducted in three stages: in-depth film characterization, nano-coat optimization, and e-coat optimization on the nano-coat.

In-Depth Film Characterization. Testing was performed to gain an understanding of the nano-coating's chemical, morphological, and growth rate characteristics on AZ91D. The chemical composition of two samples was studied via x-ray photoelectron spectroscopy (XPS), to determine if any chemical differences can account of the differences in corrosion behavior between the samples. SEM images on samples in both planar and cross-section orientation were also taken with a desire to detect morphological differences that may account for corrosion behavior, as well to assist in the development of a film growth model. A kinetics study was performed using three of the H_2ZrF_6 solutions to further assist with the same growth model. Lastly, the inductively coupled plasma (ICP) technique was performed on used H_2ZrF_6 and e-coat solutions to test for the presence of leached Mg.

XPS Characterization. XPS was performed on two of the trial runs with the H_2ZrF_6 solutions. These initial samples were at concentrations of 0.025 M and 0.100 M H_2ZrF_6 with as-diluted pH values of 1.83 and 1.67, respectively. The 0.025 M solution was used on an untreated (i.e., as-polished) AZ91D coupon, and the 0.100 M solution was tested on a two-stage acid-alkaline cleaned coupon. Both samples were analyzed with XPS for surface and bulk (~95nm sub-surface) chemistry (Table I). The surfaces of the films were very similar, showing a mix of Mg metal, $MgCO_3$, $Mg(OH)_2$, MgF_2, Al_2O_3, Al-hydroxides, ZrO_2, and ZrF_4.

Table I. Chemical composition of nano-coated specimens

		C	O	Mg	Al	Zr	F
Surface Chemistry (atomic %)	0.025 M No Pre-treat	11	50	18	2.1	2.1	14
	0.100 M Ac-Alk	9	50	20	2.6	1.3	16
Chemistry at ~95 nm (atomic %)	0.025 M No Pre-treat	4	48	23	2.1	16	8
	0.100 M Ac-Alk	2.7	42	27	2.7	6	20

The bulk of the films, however, did begin to show some of the differences between the two films. O-H bonds appear in the 0.025 M film that had received no pretreatment, that was not found in the other specimen. Likewise, the 0.100 M film with the acid-alkaline cleaning showed limited C-H-O bonding in the bulk that was not apparent in the 0.025 M film. Additional differences were found in the concentration of elements in the two films. The 0.025 M film exhibited a higher concentration of Zr and O in the bulk of the film by ~10 at% and ~6 at%, respectively, whereas the 0.100 M film was found to possess ~12 at% more F and ~4 at% more Mg than its counterpart. The bulk of the films did show some chemical similarities in the presence of both Mg and Al metal, MgO_x, MgF_2, AlO_x, ZrO_2, $Zr(OH)_4$, and ZrF_4. These results compare well with the literature, where many sources report finding similar coatings containing predominantly Zr, Mg, and Al oxides, hydroxides, hydrated oxyhydrides, and oxyfluorides [12, 16, 17].

Scanning Electron Microscopy (SEM). SEM analysis was performed on a selection of 5 samples chosen to allow the comparison of the morphological effects resulting from changes in H_2ZrF_6 concentration, solution pH, immersion time, and choice in surface pretreatment. Several common features were found in all of the films; including the presence of boulders ("massive" formations at random locations in the film), particulate matter surrounding said boulders (termed the transition zone), randomly dispersed particulate matter, and the presence of cracks in the base plane of the film.

It was observed that an increase in the concentration of H_2ZrF_6 in the coating solution decreased the size, frequency, and morphology of the boulder formations on the surface of the films. At 0.025 M H_2ZrF_6, the boulders appeared to possess a coral-like structure (Fig. 1), whereas the 0.100 M film produced boulders composed of rock-like material (Fig. 2). Additionally, the increased concentration resulted in a film with a less dense base composed of thin, cylindrical "worms" (Fig. 3) instead of the densely packed, pebble-like surface seen in the 0.025 M film (Fig. 4). Lastly, the amount of cracks present in the films was observed to decrease with the use of the higher concentration solution.

Increasing the pH also produced different coating morphologies of a more subtle nature. Raising the pH from 2.0 to 4.0 decreased the size and frequency of the boulders, as well as the size of the rocks composing the boulders. The crack severity (i.e. crack width) and number of cracks was also observed to decrease for an increase in pH. Lastly, the "worms" in the base were found to increase in diameter, and effectively increase the packing density of the base, at the elevated pH.

A markedly different coating morphology was found to occur when the immersion time was increased from 30 to 90 seconds. The base layer of "worms" was found to be significantly denser after the additional 60 seconds of immersion, as the diameter of the "worms" had greatly increased. The presence of crystallites growing from both the base and the boulders was also an additional feature of the longer immersion time (Fig. 5). Additional particulates, composed primarily of these crystallites, were observed to be randomly scattered throughout the surface of the film; appearing to grow through the base. The observed terminations of these crystallites suggests a monoclinic crystal structure, suggesting these crystals may be ZrO_2 or ZrF_4. As the energy required to form ZrO_2 (-1097 kJ/mol) is less than that for the formation of ZrF_4 (-1911 kJ/mol), it is presumed that the crystallites are ZrO_2 single crystals.

Another markedly different surface morphology was observed for a change in AZ91D surface pretreatment. An acid-alkaline two stage cleaning was observed to increase the number and size of the boulders on the film surface compared to a single stage alkaline cleaning. The two stage cleaning process also increased

the number of cracks and the amount of particulate matter on the surface. Additionally, the single stage cleaning resulted in the formation of a denser base layer. The specimen subjected to the single stage cleaning also showed the initial presence of crystallite growth on the film surface.

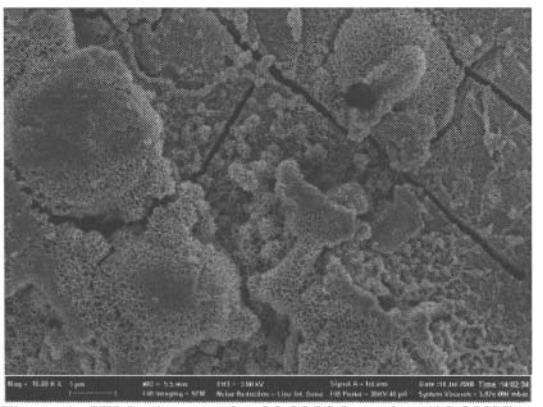

Figure 1. SEM micrograph of 0.025 M coating (10,000X)

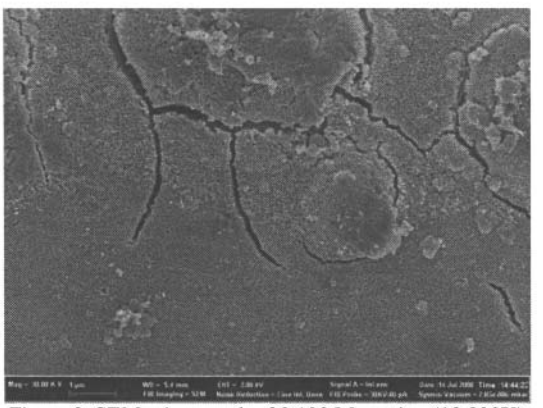

Figure 2. SEM micrograph of 0.100 M coating (10,000X)

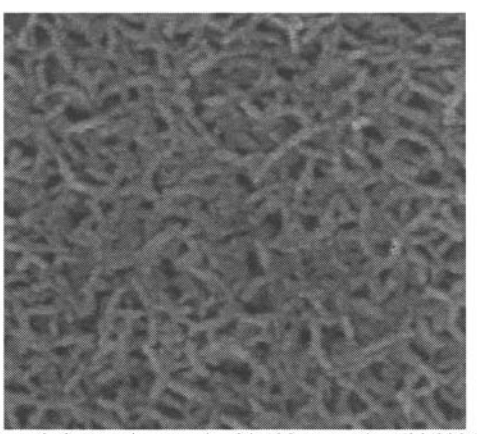

Figure 3. SEM micrograph of 0.100 M coating (30,000X)

Limited cross-section images have also been acquired (Fig. 6). These images show the presence of a two layer system on the surface of the AZ91D alloy, and also portray another difference due to the change in solution pH. Both layers were observed by electron diffraction spectrometry (EDS) to be composed of various amounts of Mg, Zr, and O, with limited amounts of F and Al present as well. Given the apparent "brightness" of the inner layer, it appears that the first layer to form is denser and contains a higher fraction of heavy elements (e.g. Zr). The outer layer, which was found to be thicker and rougher at the lower pH value, appears to contain varying concentrations of elements (chemical segregation) and the presence of multiple morphologies that may match with the topographic elements observed in the plan-view images.

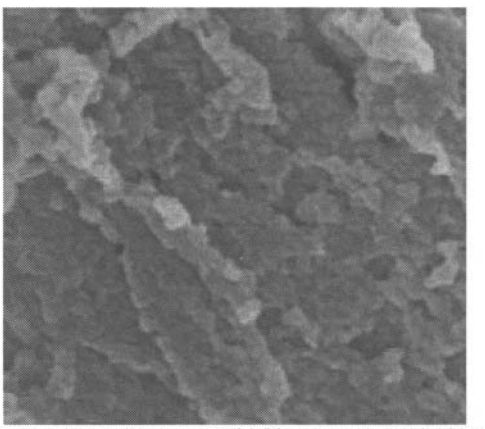

Figure 4. SEM micrograph of 0.025 M coating (30,000X

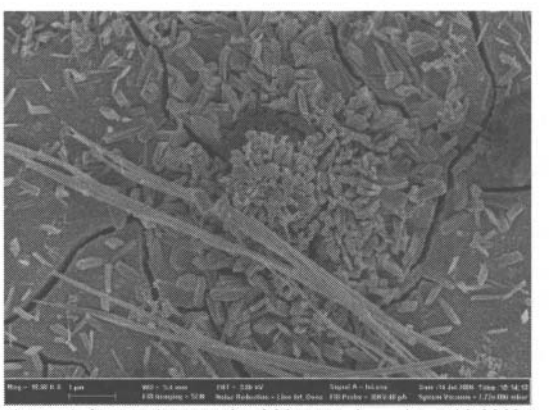

Figure 5. SEM micrograph of 90 second coating. (10,000X)

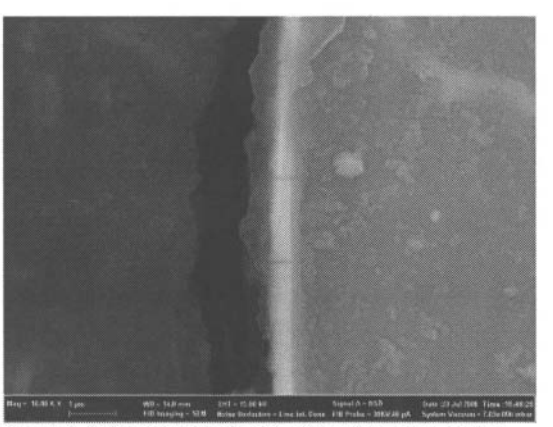

Figure 6. SEM micrograph of 4 pH coating cross-section.

Kinetics Study. Given the complex nature of the ZrO_2-based nano-coating, a better grasp of the growth mechanisms and film kinetics was desired. To accomplish this task, a standard OCP test was conducted using three different H_2ZrF_6 coating solutions: two samples that match the solutions used for the samples examined by XPS, and one sample that had an adjusted pH. In the case of the first two solutions, the AZ91D coupons were given pretreatments to match the specimens that were previously examined by XPS. The coupons tested in the 3rd solution were given an acid-alkaline two stage cleaning pretreatment. Three coupons were run for each condition for statistical purposes.

The average OCP response was calculated for the solutions from time 0 (initial immersion) to 600 seconds. First observations showed that the 0.100 M H_2ZrF_6 solutions resulted in a more noble response, indicating the presence of a more protective film being developed. The change in pH was also observed to slightly alter the OCP trace profile, but still held similar trends across the entire observation period.
Assuming that the OCP is an accurate indication of film growth, the response can be modeled using standard kinetics equations. The simplest form of the kinetics equation assumes a constant temperature:

$$V = A * \exp(k*t) \quad (1)$$

With V being the OCP (volts) at any time, t (sec), A as some initial coefficient (volts), and k is the kinetics constant (V/s). Using the average response curves for all three solutions, the coefficient, A, and the kinetics rate constant, k, were able to be calculated for the various regions that developed during the OCP measurements. It is interesting to note that the value of A was found to be roughly equal to the value of the OCP at the point in which the given region began. It was also found that a negative value for the rate constant showed periods of film growth (rising OCP) and those rate constants with positive (+) values matched with areas of film degradation (decreasing OCP).

Plotting the modeled kinetics data gathered from this analysis with the measured values shows the close correlation between the actual and the modeled values. The calculated R^2 of the models was found to be ~0.99 for all three cases, indicating that the OCP is likely measuring the film growth. This has far-reaching implications, as it may be possible to monitor film growth of all conversion coatings by following the OCP behavior, which is a simple, non-destructive test method that could be instantaneously monitored by an automated system with limited cost and minimal human interaction.

Growth Mechanisms – The OCP data from the kinetics study, coupled with SEM and XPS data, can also be used to gain a basic understanding of the film growth mechanisms. The OCP plots were observed to consist of 4 primary stages. The initial stage (Stage 0) occurs from the instant of solution contact with the Mg (time = 0) and continues for less than ½ second (Fig. 7). During this period of time the native oxide on the Mg coupon is attacked by the highly acidic coating solution [4, 13, 18, 29]. Once the native oxide has been dissolved, a magnesium-oxy-hydroxide, with the potential for a Mg-hydroxy-fluoride, deposits on the surface of the metal [9, 15, 17, 18, 27], and has been referred to as Stage I. This film continues to develop for approximately 2-4 seconds of total immersion time. As the new protective film begins to reach its growth limit, it in turn begins to be attacked by the coating solution (transition from Stage I to Stage II) [12, 15, 18, 30].

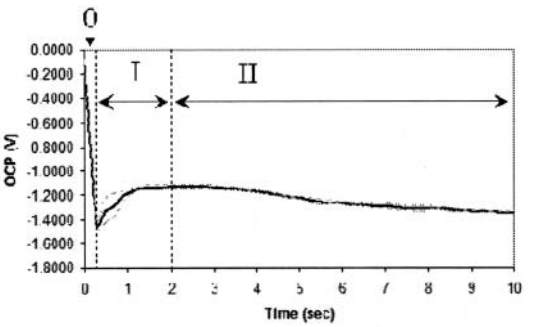

Figure 7. Average OCP response for 0.100 M, 2.1 pH coating from 0 to 10 seconds.

During this chemical attack, the film begins to accept higher concentrations of Zr, thus initiating the growth of various oxides (e.g. Al_2O_3, MgO, ZrO_2, etc.), hydroxides, and fluorides (Fig. 8) [13, 16, 19, 24, 31]. It should be noted that significant H_2 evolution was not observed until after a few seconds of immersion, further supporting the observed delay in the Zr deposition. These compounds continue to precipitate and grow on the surface of the Mg until the entire surface is fully covered (Stage II). The growth of these films continues in like fashion until the beginning of Stage III, after a total immersion time of approximately 100 seconds depending on the coating solution parameters. During the initial portions of Stage III the appearance of nano-crystallites on the surface of the film becomes apparent. Based on the SEM investigation, it appears that they initially form on the boulders, but with increased immersion time they begin to grow from or through the base of the coating as well. Based on the lack of change in the behavior of the OCP response past the onset of Stage III, it is believed that these crystals continue to grow and densify on the surface of the film with continued submersion [27].

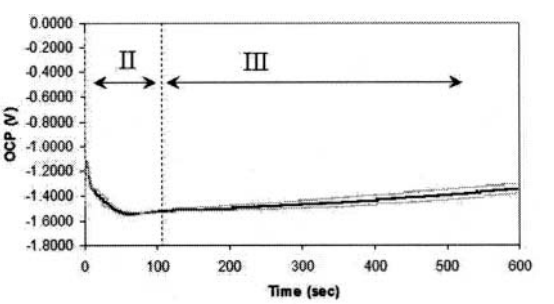

Figure 8. Average OCP response for 0.100 M, 2.1 pH coating form 0 to 600 seconds.

Fig. 9 shows the average OCP responses for all three tests. Based on these curves a few insights into the different film morphologies and growth mechanisms can be gained. By increasing the concentration of the H_2ZrF_6 solution, the OCP was found to significantly increase indicating the development of a more protective film. As magnesium fluoride is a very stable, insoluble compound, it is reasonable to assume that the addition of more F^- ions in the solution (as would be the case with increased H_2ZrF_6 concentration) would create a more dense protective film. This

was confirmed by XPS with the increased F content found in the film deposited from the higher concentration solution. An increased H_2ZrF_6 concentration was found to decrease Stage I, increase Stage II, and flatten Stage III on the OCP curves, indicating, again, that the initial protective film (Stage I) was developed more rapidly due to the increased F^- content, and takes longer times to dissolve (Stage II) in order to initiate Stage III [16].

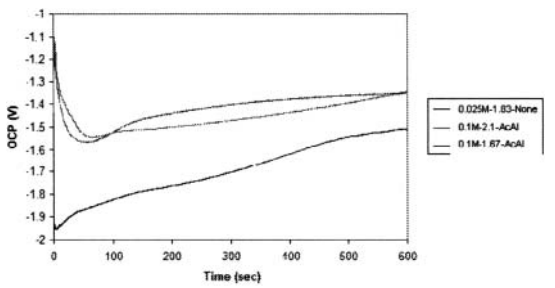

Figure 9. Average OCP response for three testing conditions.

An increase in pH was found to have a less significant impact on the film growth than was observed for a change in concentration. By increasing the pH, the only observable change was an increase in the Stage I response time, and an initial decrease in OCP values of Stage III which returned to similar values by the end of the test period, corresponding to trends observed in the literature [17]. The effects of pretreatment choice are compounded with the change in H_2ZrF_6 concentration in this series of tests, but based on the SEM observations appear to have the same general effects as a change in concentration. Namely, by choosing to use the two steps acid-alkaline cleaning treatment, there is a decrease in Stage I, increase in Stage II, and a flattening of Stage III, with an overall increase in OCP values.

Mg Dissolution Studies – The last characterization study performed on these films was used to determine how much, if any, Mg^{2+} ions were being leached into both the H_2ZrF_6 coating solution and the e-coat solution. For this portion of the investigation, the inductively coupled plasma (ICP) technique was used to measure the Mg^{2+} concentration in the H_2ZrF_6 solution after 10 runs and in the e-coat solution after 25 runs. It was found that after 10 runs in a 750 ml container, the H_2ZrF_6 solution had acquired a total Mg content of 50 ppm. Assuming equal amounts of Mg was leached into solution with each run, this averages to approximately 5 ppm per sample (each test area on the Mg coupon was approximately 2" wide by 3" long and $^1/_8$" thick). This result is promising for the use of Mg alloys with these solutions on an assembly line when compared to the 227 ppm of Mg in a phosphate solution after only one AZ91D run.

The same test was performed on an e-coat solution (1.75 liters) that was used to coat 25 samples of approximately the same size that had been coated with varying nano-coat compositions. For these 25 runs, 100 ppm of Mg was leached into the e-coat solution. Given that the e-coat solution was found to have 1.4 ppm Mg prior to any testing, the 25 coated samples added a total of approximately 98.6 ppm Mg, for an average of approximately 3.9 ppm Mg per run. It should be noted, however, that in both the H_2ZrF_6 and the e-coat solutions, there was no observable sludge or particulate buildup at the bottom of the container, or suspended in the solution. It is felt that continued research on these coatings, perhaps with the addition of a polymer in the H_2ZrF_6 solution [20, 22, 31], it may be possible to reduce the amount of Mg leached into the e-coat solution to an unobservable level.

Nano-Coat Optimization. Nano-coat optimization was conducted using the DOE discussed previously. Specimens were tested in the as-coated condition, as well as with a layer of e-coat deposited at 200 V for 3 min that had been cured at 171°C for 25 minutes. The OCP and EIS measurements of both the nano-coat single-layer, and nano-coat/e-coat bi-layer systems were acquired, the PD and coating weights gathered for the single layer nano-coat condition, and the surface roughness and adhesion values for just the bi-layer configuration.

Each response was placed into the DOE software and analyzed for statistical significance using a standard ANOVA procedure. All of the responses showed a significant statistical model could be fit to the data with varying degrees of fit (R^2). An important observation from the DOE results necessary for understanding this system is that all responses except for the e-coat adhesion show multiple parameter dependencies; further showing the complex nature of these coatings.

In addition to indicating the importance of various parameters and interactions, the more useful application of the DOE software is the calculation of a mathematical regression model to describe the measured data. These models can be used to optimize the deposition of the nano-coat to meet a series of chosen criteria. For the purposes of this project, a nano-coating was desired that minimized the corrosion current (I_{corr}) and the surface roughness (R_a); while maximizing the pore resistance (R_p), OCP_{ZrO2}, e-coat resistance (R_{el}), and e-coat adhesion (Table X). Using these criteria, a set of optimum conditions was derived by the software that would meet or exceed these demands. Using this optimized parameter set, another series of samples were made to validate the models.

Based on the results from the optimized condition, 9 of the 14 models were found to make predictions within 50% of the measured values; 3 of which were within 10% accuracy. It should be noted that given the complex nature of the variable interactions found in the ANOVA analysis, that is reasonable to assume that there are higher order interactions occurring (e.g. four-way interactions and/or cubic dependencies) that were not able to be tested due to the limited number of runs. To increase the fidelity and accuracy of the models further depositions and testing should be performed. Based on the available data, however, it can be stated that the nano-coating deposition is not a simple, linear process, but rather a very complex interaction with a multitude of competing forces.

E-coat Optimization. Using the optimized ZrO_2-based nano-coating as the base layer, a second DOE was developed (as discussed above) to optimize the addition of an e-coat layer for increased corrosion protection, and to present a surface ready for paint application. The responses were coating thickness, $OCP_{e\text{-}coat}$, EIS, surface roughness, and e-coat adhesion. As with the nano-coat DOE, all of the variables in this second series of experiments were able to be statistically modeled. In all but one of the cases, there was a complex parabolic interaction. The only case where this trend was not observed was for the OCP, which resulted in an R^2 of 0.246 indicating that the model does not accurately match the available data. Several of the other R^2

values are also questionable (i.e. C_{el}, R_{el}, and roughness), but are still within an acceptable range. The reason for these low R^2 values may be the presence of higher order variable dependencies (e.g. t^3 and/or V^3) that could not be analyzed with the selection of samples processed.

Optimization of the bi-layer system of e-coat on the nano-coat base layer was determined by minimizing the surface roughness to a value less than 45 nm and maximizing the OCP, R_{el}, and adhesion. The resulting optimized condition was found to be 150 V for 3 minutes, which was one of the runs tested for the DOE. Comparing the predicted values from the models back to the original run data showed that all predicted values were within 15% of the measured data. Given the sub-standard R^2 values associated with the models, this agreement between data and models is a good indication of the model's ability for optimization.

Summary

Investigations have been performed on the coating mechanisms of a ZrO_2-based nano-coating on Mg alloy AZ91D. A basic film growth model has been developed based on the morphologies observed in the SEM and the profiles gathered via the monitoring of OCP during deposition. The stages of the models are related to the chemistries found to be present in the films by XPS. Preliminary tests were also performed to determine that a small amount of Mg was being leached into the conversion coating solution (~5 ppm per samples) and the e-coat solution (~4 ppm per sample). Two series of DOE experiments were also conducted to optimize 1). the deposition of the ZrO_2-based nano-coating (at a concentration of H_2ZrF_6 of 0.100 M, solution pH of 2.10, and acid-alkaline two-stage pretreatment for 35 seconds), and 2). the e-coat that was deposited on top of the optimized ZrO_2-based coating (at 150 V for 3 minutes). The work has shown that the use of ZrO_2-based nano-coatings on Mg alloy AZ91D improves the corrosion resistance of the base metal, and that the use of e-coat on top of the nano-coating greatly improves the component's corrosion resistance. The final optimized sample (with optimum nano-coat and e-coat depositions) showed a smooth, adherent, and well protected magnesium component.

Acknowledgements

The authors would like to thank Sundaresan Avudaiappan for training James on the use of appropriate equipment for the necessary testing. Curt Wong for operating the SEM. Steve Gaarenstroom and Maria Militello for XPS and ED-XRF testing and analysis, and Nick Irish for the ICP work. Willie Dixon for sectioning the Mg plates, and for training on the appropriate sample preparation and polishing equipment.

References

1. Gray, J. and B. Luan, *Protective coatings on magnesium and its alloys—a critical review.* Journal of Alloys and Compounds, 2002. **336**(1-2): p. 88-113.
2. Ardelean, H., I. Frateur, and P. Marcus, *Corrosion protection of magnesium alloys by cerium, zirconium and niobium-based conversion coatings.* Corrosion Science, 2008.
3. Zhai, Y., et al., *A Replacement for Phosphate Conversion Coating Based on Hexafluorozirconic Acid.* 2008.
4. Zhou, W., et al., *Structure and formation mechanism of phosphate conversion coating on die-cast AZ91D magnesium alloy.* Corrosion Science, 2008. **50**(2): p. 329-337.
5. Gao, G. and M. Ricketts, *Evaluation of Protective Coatings on Magnesium for Phosphate Process Compatibility and Galvanic Corrosion Prevention.* 2002.
6. Giles, T., et al., *New Generation Conversion Coatings for the Automotive Industry.* 2007.
7. Talbert, R. (2007) *Pretreatments: The Next Generation.* **Volume**,
8. Zhao, M., et al., *Influence of surface pretreatment on the chromium-free conversion coating of magnesium alloy.* Materials Chemistry & Physics, 2007. **103**(2-3): p. 475-483.
9. Elsentriecy, H., K. Azumi, and H. Konno, *Effect of surface pretreatment by acid pickling on the density of stannate conversion coatings formed on AZ91 D magnesium alloy.* Surface & Coatings Technology, 2007. **202**(3): p. 532-537.
10. Maddela, S., et al., *Cerium-Based Conversion Coating on AZ91D Alloy-II.* 2008.
11. Maddela, S., et al., *Preliminary Studies of Cerium Based Conversion Coatings on AZ91D Alloy.* 2008.
12. Gray, J. and B. Luan, *Protective coatings on magnesium and its alloys□a critical review.* Journal of Alloys and Compounds, 2002. **336**(1-2): p. 88-113.
13. Knudsen, O.O. and A. Bjorgum, *Chromium free pretreatments - state of the art.* unknown.
14. Skar, J., L. Sivertsen, and J. Öster, *Chrome-free Conversion Coatings for Magnesium Die Castings□a Review.* ICEPAM-International Conference on Environmental friendly pre-treatment for Aluminum and other Metals, Oslo, Norway, 2004.
15. Walter, M., *Magpass-CoatSr as a Chrome-Free Pre-Treatment for Paint Layers and An Adhesive Primer for Subsequent Bonding.* 2004.
16. Verdier, S., et al., *Monochromatized x-ray photoelectron spectroscopy of the AM60 magnesium alloy surface after treatments in fluoride-based Ti and Zr solutions.* Surf. Interface Anal, 2005. **37**: p. 509-516.
17. Verdier, S., et al., *An electrochemical and SEM study of the mechanism of formation, morphology, and composition of titanium or zirconium fluoride-based coatings.* Surface & Coatings Technology, 2006. **200**(9): p. 2955-2964.
18. Verdier, S., et al., *The surface reactivity of a magnesium□aluminium alloy in acidic fluoride solutions studied by electrochemical techniques and XPS.* Applied Surface Science, 2004. **235**(4): p. 513-524.
19. Lunder, O., et al., *Formation and characterisation of Ti□Zr based conversion layers on AA6060 aluminium.* Surface & Coatings Technology, 2004. **184**(2-3): p. 278-290.
20. Mirabedini, S., et al., *Characterization and Corrosion Performance of Powder Coated Aluminium Alloy.* IRANIAN POLYMER JOURNAL, 2003. **12**: p. 261-270.
21. Nickerson, B.C. and E. Lipnickas, *Characterization of A Viable Non-Chromated Conversion Coating Aluminum and its Alloys by Electrochemical and Other Methods.* unknown.
22. Reghi, G.A., *Process for corrosion resisting treatments for aluminum surfaces.* 1992, US Patent 5,089,064.
23. Reghi, G.A., *IMPROVED CHROMIUM-FREE COMPOSITION AND PROCESS FOR CORROSION RESISTING TREATMENTS FOR ALUMINUM SURFACES.* 1994, EP Patent 0,555,383.
24. Schram, T., G. Goeminne, and H. Terryn, *Study of the composition of zirconium- based chromium free conversion layers on aluminum [JI Trans. Inst.* Metal Finishing, 1995. **73**: p. 91-95.

25. Puomi, P., et al., *Optimization of commercial zirconic acid based pretreatment on hot-dip galvanized and Galfan coated steel.* Surface & Coatings Technology, 1999. **115**(1): p. 79-86.
26. Romero Pareja, R., et al., *Corrosion behaviour of zirconia barrier coatings on galvanized steel.* Surface & Coatings Technology, 2006. **200**(22-23): p. 6606-6610.
27. Stromberg, C., et al., *Synthesis and characterisation of surface gradient thin conversion films on zinc coated steel.* Electrochimica Acta, 2006. **52**(3): p. 804-815.
28. Tepe, B. and B. Gunay, *Evaluation of pre-treatment processes for HRS (hot rolled steel) in powder coating.* Progress in Organic Coatings, 2007.
29. Ambat, R., N. Aung, and W. Zhou, *Evaluation of microstructural effects on corrosion behaviour of AZ91D magnesium alloy.* Corrosion Science, 2000. **42**(8): p. 1433-1455.
30. Say, W., C. Chen, and S. Hsieh, *Electrochemical characterization of non-chromate surface treatments on AZ80 magnesium.* Materials Characterization, 2008.
31. Nordlien, J., et al., *Formation of a zirconium-titanium based conversion layer on AA 6060 aluminium.* Surface & Coatings Technology, 2002. **153**(1): p. 72-78.